REVIEWS

*Journal of Semiconductors*
(2023) 44, 031001
doi: 10.1088/1674-4926/44/3/031001

# Preparation, properties, and applications of $Bi_2O_2Se$ thin films: A review

**Huayu Tao[1, 2], Tianlin Wang[1], Danyang Li[1], Jie Xing[1], and Gengwei Li[1, †]**

[1]School of Science, China University of Geosciences, Beijing 100083, China

[2]School of Materials Science and Technology, China University of Geosciences, Beijing 100083, China

**Abstract:** Two-dimensional materials have shown great application potential in high-performance electronic devices because they are ultrathin, have an ultra-large specific surface area, high carrier mobility, efficient channel current regulation, and extraordinary integration. In addition to graphene, other types of 2D nanomaterials have also been studied and applied in photodetectors, solar cells, energy storage devices, and so on. $Bi_2O_2Se$ is an emerging 2D semiconductor material with very high electron mobility, modest bandgap, near-ideal subthreshold swing, and excellent thermal and chemical stability. Even in a monolayer structure, $Bi_2O_2Se$ has still exhibited efficient light absorption. In this mini review, the latest main research progresses on the preparation methods, electric structure, and the optical, mechanical, and thermoelectric properties of $Bi_2O_2Se$ are summarized. The wide rang of applications in electronics and photoelectronic devices are then reviewed. This review concludes with a discussion of the existing open questions/challenges and future prospects for $Bi_2O_2Se$.

**Key words:** two-dimensional material; $Bi_2O_2Se$; electronical structure; optical property; thermoelectricity

**Citation:** H Y Tao, T L Wang, D Y Li, J Xing, and G W Li, Preparation, properties, and applications of $Bi_2O_2Se$ thin films: A review[J]. *J. Semicond.*, 2023, 44(3), 031001. https://doi.org/10.1088/1674-4926/44/3/031001

## 1. Introduction

Two-dimensional (2D) materials have attracted much attention due to their ultrathin atomic layer thickness, tunable band structures, super large specific surface area, good mechanical flexibility, and rich physical and chemical properties. In the last decade, great progress has been made in the application of 2D materials in the next generation of electronics, optoelectronics[1–3], sensors[4–6], energy storage device[7], and flexible electronics[8]. As an allotrope of carbon, graphene is the earliest-found and most popular 2D material (Figs. 1(a)–1(c)). It has excellent electrical, thermal, optical, and mechanical properties, and therefore has wide application in the fields of information, energy, medical treatment, military, and so on[9]. However, as a leading member of the 2D material family, single-layer graphene has a zero-optical bandgap, which greatly limits its applications in semiconductor logic devices, storage, and photocatalysis. Moreover, the monolayer graphene only absorbs 2.3% of incident light power. Therefore, researchers have turned their attention to other 2D nanomaterials, such as black phosphorus[10–12] and transition metal chalcogenides (TMDCs)[13], and so on. Black phosphorus (Fig. 1(d)) has high carrier mobility (~1000 $cm^2/(V{\cdot}s)$ at room temperature) and anisotropic mechanical and electrical transport properties; however, its environmental instability is challenging for its practical application in air. TMDCs (Fig. 1(e)) represent a large family with a chemical formula of $MX_2$, where M is a transition metal atom and X is a chalcogen atom. Most TMDCs with atomically thickness exhibit direct bandgap, strong spin-orbit coupling, fairly high mobility, and favorable electronic and optical properties. Following the research upsurge of graphene, black phosphorous, and transition metal dichalcogenides, multiple-element layered 2D materials have become a new research focus due to their more abundant structure and more diversified characteristics. Therefore, it is interesting and significant to find ternary or even multi-element 2D materials and explore their possibility in future applications.

Recently, $Bi_2O_2Se$, as a ternary layered Bi-based oxychalcogenide material semiconductor material, has attracted much attention. $Bi_2O_2Se$ has a modest bandgap of 0.8 eV, high mobility (1.9 K, 29 000 $cm^2/(V{\cdot}s)$, room temperature, 450 $cm^2/(V{\cdot}s)$) and good thermal and chemical stability[11]. $Bi_2O_2Se$ possesses a tetragonal crystal structure, with $[Bi_2O_2]_n^{2n+}$ and $[Se]_n^{2n-}$ layer stacking alternatively. Due to its interlayered zipper-like structure, it exhibits unique characteristics[16]. In contrast to other van der Waals 2D layered materials, the layers of $Bi_2O_2Se$ are connected by relatively strong electrostatic forces. Therefore, special exfoliation method or growth strategy is developed to fabricate large-area and atomically thick $Bi_2O_2Se$ thin films. In view of these stable, unique, and excellent properties, $Bi_2O_2Se$ can be used for promising applications in integrated circuits[17–19], optoelectronics[20–22], thermoelectrics[23], neuromorphic computing[24, 25], and so on.

In this review, we will briefly summarize the recent research progress of $Bi_2O_2Se$. First, the preparation methods, optical, mechanical, and thermoelectric properties are summarized. Then the applications as photodetectors (transistors), energy storage devices, memristors, optical switches, and biomedical devices are then elaborated. Finally, the existing open questions and prospects of $Bi_2O_2Se$ are presented.

## 2. Preparation methods

A controllable preparation process of large-area and high-quality 2D $Bi_2O_2Se$ thin films is the prerequisite for the ap-

Correspondence to: G W Li, ligw@cugb.edu.cn
Received 22 AUGUST 2022; Revised 3 OCTOBER 2022.

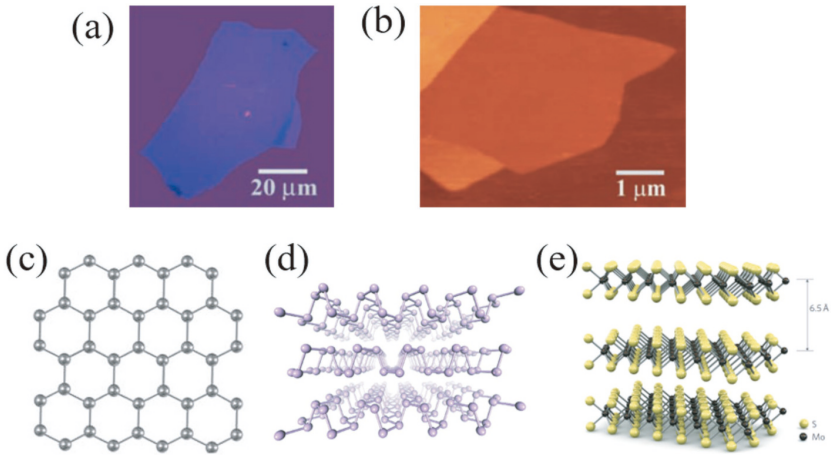


Fig. 1. (Color online) (a) Graphene optical photographs with a thickness of about 3 nm. (b) Atomic force microscope images of monolayer graphene. Reproduced with permission[9]. Copyright 2004, The American Association for the Advancement of Science. (c) Schematic diagram of the atomic structure of graphene. (d) Schematic diagram of black phosphorus atomic structure. Reproduced with permission[14]. Copyright 2014, Nature Publishing Group. (e) Schematic diagram of $MoS_2$ atomic structure. Reproduced with permission[15]. Copyright 2011, Nature Publishing Group.

Table 1. Summary of preparation methods, growth conditions, and basic characteristics for $Bi_2O_2Se$.

| Method | Precursor, growth conditions | Domain size ($\mu$m) | Thickness (nm) | Mobility ($cm^2/(V{\cdot}s)$) | Ref. |
|---|---|---|---|---|---|
| CVD | $Bi_2Se_3$, $Bi_2O_3$, 600–640 °C, 400 Torr | ~200 | 2–4 layers | ~313 (300 K)–20660 (2 K) | [31] |
| CVD | Se, $Bi_2O_3$, 680 °C, 400 Torr | ~250 | 4 layers | 410 (RT) | [32] |
| CVD | $Bi_2Se_3$,$Bi_2O_3$, 580–650 °C, 100-400 Torr | >200 | 6.7 | ~450 (RT)–29000 (1.9 K) | [11] |
| CVD | $Bi_2Se_3$, $Bi_2O_3$, 550–630 °C, 30 Pa | ~180 | 9.8 | 98 (300 K) | [33] |
| CVD | $Bi_2Se_3$, $Bi_2O_3$, 620 °C, 350–400 Torr | ~100 | 5.2 | 107 | [34] |
| CVD | $Bi_2Se_3$, $Bi_2O_3$, <670 °C | ~200 | 0.65 | ~262 (RT) | [35] |
| CVD | $Bi_2Se_3$, $Bi_2O_3$, >670 °C | >1700 | 10.8 | – | [35] |
| Reverse-flow CVD | $Bi_2O_2Se$ powder, 760 °C, 400 mbar | ~750 | 13.7 | 1400 (RT) | [47] |
| Modified Bridgman method | $Bi_2O_3$, Se, Bi powder | Bulk | Bulk | $2.8 \times 10^5$ (2 K) | [37] |
| Hydrothermal method | $C_6H_{13}BiN_2O_7{\cdot}H_2O$, $Na_2O_3Se$ and KOH | >2 | 4.7 | – | [48] |
| Hydrothermal method | $Na_2SeO_3$, $C_6H_{13}BiN_2O_7{\cdot}H_2O$ and KOH | >60 | 4.92 | 334.7 (RT) | [49] |
| Solution-assisted method | $Bi(NO_3)_3{\cdot}5H_2O$, $(CH_2OH)_2$, 500 °C, 400 Torr | Continuous | 8.5 | 74 (RT) | [18] |

plication of electronic devices. Generally, the preparation methods of 2D materials are mainly divided into two categories: the top-down method and the bottom-up method. The top-down method is to obtain 2D thin films by peeling from bulk materials by chemical or mechanical means, including mechanical cleavage method, electrochemical Li-intercalation and exfoliation, Li-intercalation and exfoliation with n-butyllithium, and so on[26–30]. The production of TMDCs monolayers is usually achieved by micromechanical exfoliation of large crystals from top to bottom[9]. In theory, the mechanical exfoliation method can obtain thin films with high-quality, high-purity, and uniform thickness, which can be used to prepare electronic devices. However, this method has low repeatability and cannot effectively control the thickness and size of thin films. To improve reproducibility and controllability, a bottom-up method is needed to synthesize high-quality and large-area 2D single-crystal thin films. So far, many methods have been used to prepare more stable and high-quality $Bi_2O_2Se$ single crystal, such as chemical vapor deposition (CVD)[11, 31–36], modified Bridgman method[22, 37], wet chemical synthesis, hydrothermal reactions[27, 38], and so on. The bottom-up method can be used to grow $Bi_2O_2Se$ single crystal directly on the target substrate by precisely controlling the growth conditions. Therefore it has more freedom to optimize the growth and improve the film quality. Table 1 summarizes the preparation methods, growth conditions, and basic film characteristics for $Bi_2O_2Se$ reported in the literature.

### 2.1. CVD growth

Chemical vapor deposition (CVD) is a common bottom-up method to fabricate 2D materials, in which a variety of growth parameters, such as heating temperature, gas pressure, precursor concentration, gas flow rate and so on, are needed to be optimized to realize the growth of atomically thin 2D film[39]. In this process, gaseous compounds are formed first and transported by inert gas to the target substrate, as shown in Fig. 2(a). High-quality $Bi_2O_2Se$ single crystal thin films with adjustable size, controllable thickness, and excellent electronic properties can be prepared by CVD method[11, 20, 40–42]. In the early stages, Wu *et al.* and Li *et al.* synthesized 2D $Bi_2O_2Se$ crystals with large area, high mobility, and thin film on mica ($[KMg_3(AlSi_3O_{10})F_2]$) using $Bi_2O_3$ and $Bi_2Se_3$ as precursors as shown in Fig. 2(b)[31, 41]. It has been confirmed that the nucleation sites, thickness, domain sizes, and crystal phase transition of $Bi_2O_2Se$ thin films can be well controlled by adjusting growth conditions (Figs. 2(c)–2(f)). For example, by controlling the temperature, planar and vertical $Bi_2O_2Se$ nanosheets can be synthesized as shown in Figs. 2(g)

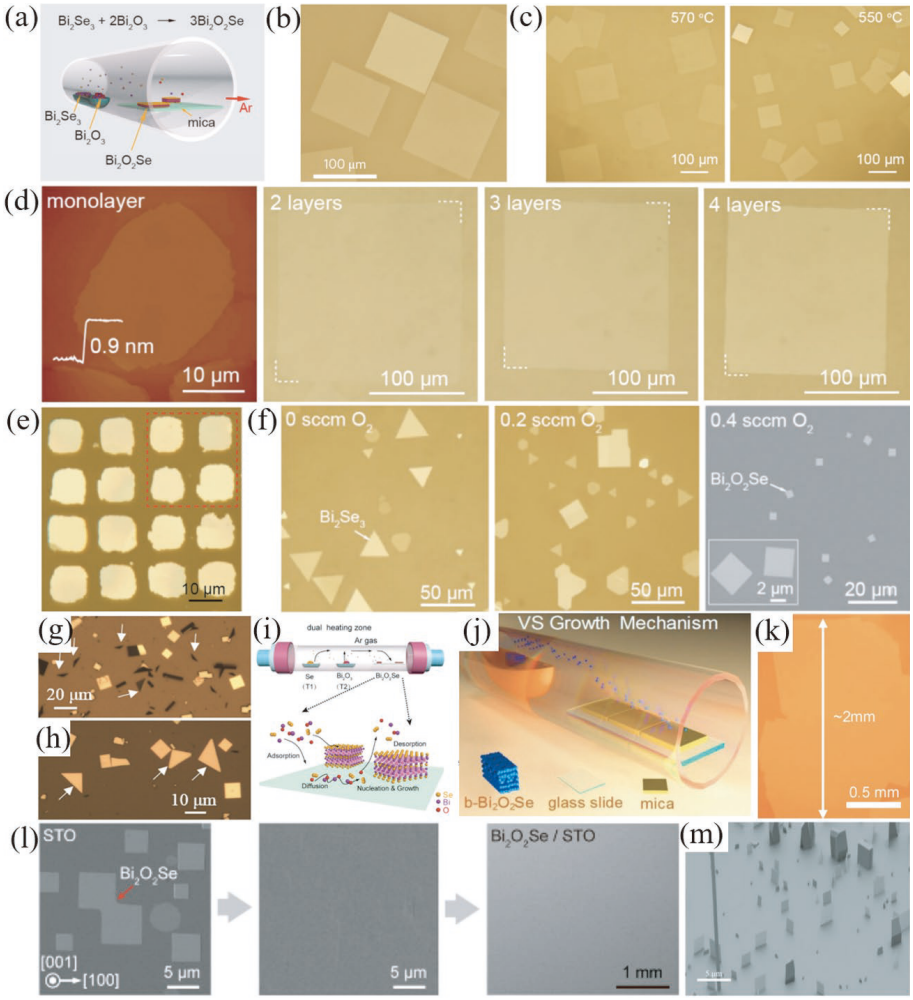


Fig. 2. (Color online) Preparation of two-dimensional films by CVD method. (a) CVD preparation diagram. Reproduced with permission[31]. Copyright 2017, American Chemical Society. (b) 2D $Bi_2O_2Se$ crystal synthesized on mica. Reproduced with permission[11]. Copyright 2017, Nature Publishing Group. (c–f) Domain size and crystal phase transition of $Bi_2O_2Se$ thin films. Reproduced with permission[31]. Copyright 2017, American Chemical Society. (g, h) SEM of both transverse $Bi_2O_2Se$ and vertical triangular $Bi_2O_xSe$. Reproduced with permission [41]. Copyright 2018, Wiley-VCH. (i) Improved preparation method. Reproduced with permission[32]. Copyright 2019, American Chemical Society. (j, k) Schematic of VS growth mechanism. Reproduced with permission[20]. Copyright 2019, Wiley-VCH. (l) SEM pictures of $Bi_2O_2Se$ on STO. Reproduced with permission[19]. Copyright 2019, American Chemical Society. (m) Vertical growth of 2D $Bi_2O_2Se$ films. Reproduced with permission[43]. Copyright 2019, Wiley-VCH.

and 2(h). At lower temperatures, a kinetics-dominated growth was met. Precursors tend to get rid of the restriction of the substrate and grow into the vertical direction. At higher growth temperatures, only $Bi_2O_2Se$ with the lateral layout was grown, which is a thermodynamics-controlled growth process due to higher migration rate of adatoms[41, 43].

Carrier concentration is one of the most important parameters for semiconductor materials. In field effect transistors, the low carrier concentration of the channel can induce good gating, which is very important for reducing the operating voltage to manufacture low-power digital devices. However, when using $Bi_2O_3$ and $Bi_2Se_3$ as precursors, $Bi_2Se_3$ is firstly decomposed according to $Bi_2Se_3(s) = 2BiSe(g) + \frac{1}{2} Se_2(g)$, and the decomposition may change greatly after prolonged heating, which will adversely affect the synthesis of 2D $Bi_2O_2Se$ crystals, resulting in higher residual carrier concentration.

To eliminate the possible side reactions, defects, or vacancies, Wu *et al.* synthesized $Bi_2O_2Se$ crystals using Se element and $Bi_2O_3$ powder as precursors through a two-temperature zone heating system. The fabricated $Bi_2O_2Se$ film has an ultra-low residual carrier concentration of $10^{16}$ $cm^{-3}$ and high Hall carrier mobility up to 410 $cm^2/(V{\cdot}s)$ at room temperature (Fig. 2(i))[32]. Compared with the complex and changeable decomposition reactions of $Bi_2Se_3$, Se elements mainly volatilize into single $Se_2$ molecules. The dual heating zone system can change the relative partial pressure of Se and Bi precursors by controlling the heating temperature of Se and $Bi_2O_3$ sources separately. Finally, by optimizing the growth conditions, the defects or vacancies that lead to the n-type conductivity of $Bi_2O_2Se$ can be greatly reduced, thus reducing the carrier concentration by 2–3 orders of magnitude. In previous reports, the size of the synthesized $Bi_2O_2Se$ flakes is mostly at the micron scale. Wu *et al.* developed a new self-limiting vapor-solid (VS) deposition method to achieve the growth of millimeter 2D $Bi_2O_2Se$ thin films on a mica substrate, in which $Bi_2O_2Se$ powder as the sole growth source was put in a tubular furnace under normal pressure as shown in Figs. 2(j) and 2(k), and the $Bi_2O_2Se$ powder can be synthesized by hydrothermal method or CVD method[20].

Because the Bi-O layers in $Bi_2O_2Se$ are structurally compat-

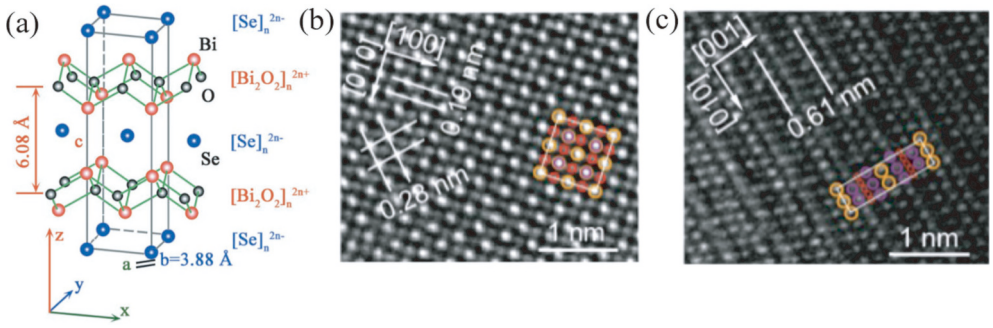


Fig. 3. (Color online) (a) Crystal structure of $Bi_2O_2Se$. Reproduced with permission[46]. Copyright 2018, Wiley-VCH. (b, c) HRTEM of $Bi_2O_2Se$. Reproduced with permission[31]. Copyright 2017, American Chemical Society.

ible with many perovskite oxides, and it exhibits rich and interesting physical properties (e.g, ferroelectricity, magnetism, thermoelectricity, etc.). Tan *et al.* synthesized $Bi_2O_2Se$ on perovskite oxide by the CVD method and studied the growth process as shown in Fig. 2(l), which provides an alternative platform for studying new physical phenomena of oxide heterostructures[19].

Due to the good lattice matching and good thermal stability, mica substrate is commonly used in the CVD growth of 2D $Bi_2O_2Se$. However, thanks to the strong binding force between mica substrate and $Bi_2O_2Se$ thin films, it is difficult to transfer $Bi_2O_2Se$ thin films to the new substrate to prepare the devices for the following measurement. In the application of 2D $Bi_2O_2Se$ to electronic devices, $SiO_2$/Si substrate has usually been used as a support for 2D materials. In transmission electron microscopy (TEM) characterization, $Bi_2O_2Se$ needs to be transferred to a copper grid. It also requires a safety transfer method that could minimize the damage to $Bi_2O_2Se$ as small as possible and at the same time is convenient to manipulate. Fu *et al.* used Raman spectroscopy to demonstrate the inevitable damage to $Bi_2O_2Se$ when using hydrofluoric acid (HF) in the wet transferring. The authors developed a polystyrene (PS)-assisted noncorrosive transfer method. PS was firstly spin-coated onto the surface of f-mica and then baked. Subsequently, the PS film together with $Bi_2O_2Se$ was peeled away from the f-mica with the assistance of deionized (DI) water. After this unique transfer method, the performance of $Bi_2O_2Se$ devices is greatly improved[34]. Khan *et al.* used a polydimethylsiloxane (PDMS) and poly(methyl methacrylate) (PMMA)-assisted method to transfer $Bi_2O_2Se$ flakes grown on mica substrate synthesized by VS deposition. Nevertheless this method is only effective in detaching thick $Bi_2O_2Se$ flakes from mica[20, 44]. Chen *et al.* developed a method to transfer $Bi_2O_2Se$ sheets using PDMS only, which is proved to be a more convenient and effective method to transfer thinner $Bi_2O_2Se$ flakes[44].

Wu *et al.* introduced $Bi_2O_3$ as a seed layer and realized the vertical growth of 2D $Bi_2O_2Se$ films on mica substrate by the CVD method, as shown in Fig. 2(m)[43]. These vertically grown $Bi_2O_2Se$ thin films can be easily and cleanly transferred to the target substrate. Zhang *et al.* proposed a simple, rapid, and extensible solution-assisted method to synthesize high-quality $Bi_2O_2Se$ thin films on flexible muscovite substrates through the decomposition of $Bi(NO_3)_3{\cdot}5H_2O$ precursor and the following selenization. By changing the rotation speed of precursor solution, the thickness of the $Bi_2O_2Se$ thin films can be accurately controlled to a few atomic layers[18]. However, due to the strain caused by limited growth temperature and the softness of the substrate, the electronic property of flexible device performance is usually poorer than that on rigid substrates.

### 2.2. The modified Bridgman method

Bridgman invented the crucible descent method in 1925, which was called the Bridgman method. Later, Stockbarger developed this method and named it as the B-S method, which is one of the most commonly used methods for preparing large-size single crystals. The brief preparation process is as follows: the precursor materials needed for crystals growth are placed in a cylindrical crucible and slowly lowered. The furnace temperature is controlled slightly above the melting point of the material through a heating furnace with a certain temperature gradient. When the crucible passes through the heating zone, the materials in the crucible are melted. When the crucible continues to fall, the temperature at the bottom of the crucible first drops below the melting point and starts to crystallize, and the crystals continue to grow as the crucible falls down. This method has many advantages. First, the shape of the crystals grown depends on the crucible, and the shape of the crucible can be designed according to the needs. Second, it is suitable for growing large-size single crystals and multiple crystals. Finally, the growth method is simple and easy to operate, which is convenient for automation and industrialization. Xu *et al.* and Chen *et al.* successfully synthesized uniform and high-quality $Bi_2O_2Se$ single crystals in a vacuum quartz tube using $Bi_2O_3$, Se, and Bi powders as precursors by a modified Bridgman method[22, 37].

### 2.3. Hydrothermal method

The hydrothermal method is also known as a high-pressure solution method. This method uses high-temperature and high-pressure aqueous solutions to dissolve or react substances that are insoluble or difficult to dissolve in water under atmospheric conditions to form a dissolved product of the substance and then crystallize and grow after reaching a certain degree of supersaturation. The hydrothermal method has the characteristics of mild reaction conditions, convenient and simple operation, the synthesized crystals have few defects, high uniformity, and high purity[45]. Tian *et al.* synthesized $Bi_2O_2Se$ crystals by hydrothermal method using deionized water, hydrazine hydrate ($N_2H_4{\cdot}H_2O$), NaOH, Se powder, $Bi(NO_3)_3{\cdot}5H_2O$, $LiNO_3$ powder, and $KNO_3$ powder as raw materials[46]. Chen[21] and Khan *et al.*[20] also synthesized bulk $Bi_2O_2Se$ by hydrothermal method using deionized water, $LiNO_3$, $KNO_3$, $Bi(NO_3)_3{\cdot}5H_2O$, Se, and $N_2H_4{\cdot}H_2O$ as precursors.

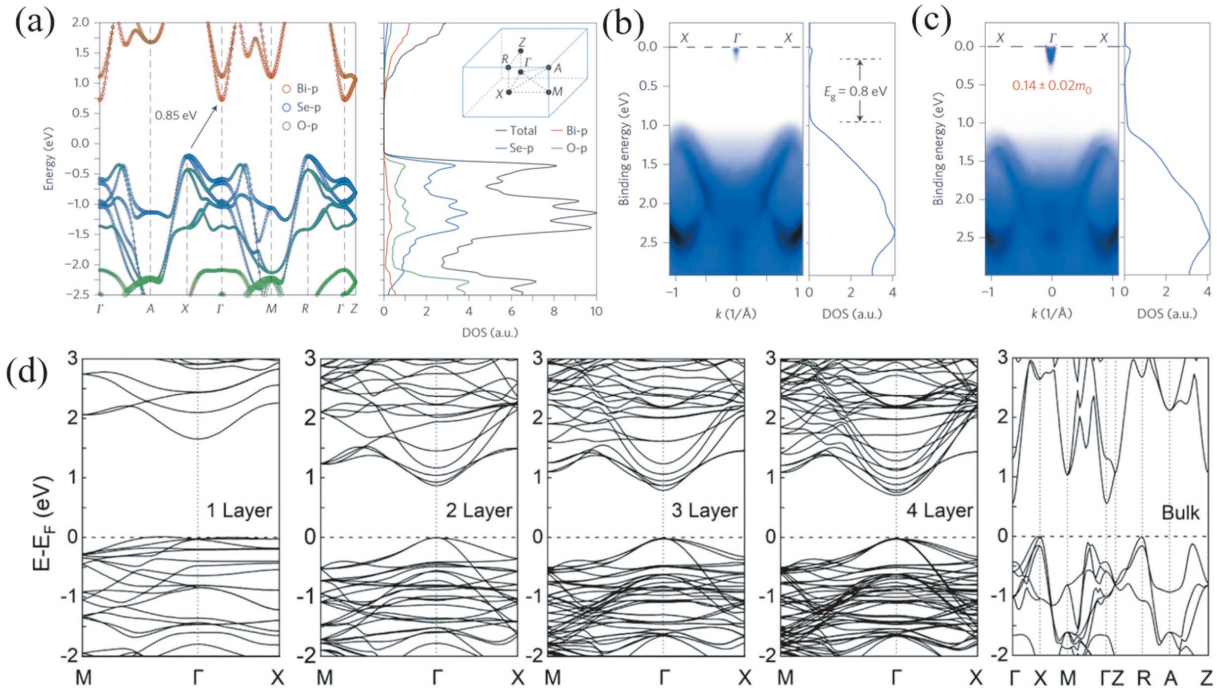


Fig. 4. (Color online) (a–c) ARPES of $Bi_2O_2Se$ films. Reproduced with permission[11]. Copyright 2017, Nature Publishing Group. (d) Band structure of $Bi_2O_2Se$ films and bulk. Reproduced with permission[16]. Copyright 2019, Nature Publishing Group.

## 3. Properties and characterizations

### 3.1. Crystal structure

2D layered material $Bi_2O_2Se$ is a typical bismuth-based oxychalcogenide material with a layered structure. As shown in Fig. 3(a)[46], the 4-fold symmetric $Bi_2O_2Se$ has a tetragonal crystal structure and belongs to I4/mmm space group ($a$ = $b$ = 3.8 Å, $c$ = 12.16 Å), in which there are 10 atoms in the unit cell[37, 50], and the monolayer thickness of $Bi_2O_2Se$ is about 0.61 nm[32, 33]. Wu *et al.* confirmed the single crystal structure and monolayer thickness of $Bi_2O_2Se$ by high-resolution transmission electron microscopy (HRTEM)[31]. As shown in Figs. 3(b) and 3(c), the obtained lattice spacing of 0.19, 0.28 nm, and the layer spacing along the [001] direction of 0.61 nm is consistent with the theoretical values. Bi, O and Se atoms located at Wyckoff positions of 4e (0,0,$z$), 4d (0,1/2,1/4) and 2a (0,0,0), respectively. Therefore, the only free atomic coordinate in the structure is the $z$ coordinate of the Bi atom. In the crystal structure, Bi atoms and O atoms form $Bi_2O_2$ layers perpendicular to [001] direction, and Se atoms form atomic layers located between the $Bi_2O_2$ layers. $Bi_2O_2Se$ has a repeating sequence of ...-$(Bi_2O_2)_1$-$Se_1$-$(Bi_2O_2)_2$-$Se_2$-... layers[37]. For the $Bi_2O_2Se$ nanosheet, the distance between Bi and Se (3.18 Å) is much larger than the sum of the effective ion radius of $Bi^{3+}$ (~1.03 Å) and $Se^{2-}$ (~1.98 Å) but is shorter than that in bulk $Bi_2O_2Se$ (3.27 Å). However, the Bi–O bond length (2.37 Å) is longer than that in bulk $Bi_2O_2Se$ (2.31 Å). The results indicate that in the $Bi_2O_2Se$ nanosheet the Bi–O bond is weaker while the interaction between Bi and Se layers is stronger than that in the bulk, which is conducive to the stability of the $Bi_2O_2Se$ nanosheet[46, 51, 52]. In addition, the 2D square lattice formed by Bi-Bi with a distance of 3.8 Å in the $[Bi_2O_2]_n^{2n+}$ layer is structurally compatible with many perovskite oxides and their heterostructure shows rich and interesting physical characteristics (ferroelectricity, magnetism, and high-$T_c$ superconductivity)[9]. $Bi_2O_2Se$ had very high stability and no phase transition occurred below 30 GPa[53].

### 3.2. Electronic structure and optical property

Unlike other 2D semiconductor materials, layered $Bi_2O_2Se$ lacks the standard van der Waals gap[16]. Consequently, it can be cleaved along the Se plane and the atomic structure may be rearranged at the surface, indicating the existence of nonequilibrium electrons distributed between $[Bi_2O_2]_n^{2n+}$ and $[Se]_n^{2n-}$. Wu *et al.* combined the first-principle calculations and angle-resolved photoemission spectroscopy (ARPES) measurement to study the band structure and state density of bulk $Bi_2O_2Se$ (Fig. 4). The minimum value of the conduction band (CBM) and the maximum value of the valence band (VBM) are located at points Γ and X, respectively, revealing its indirect band gap. The bands near CBM are very steep, while those near VBM are relatively flat[54]. By fitting the conduction band, a very low in-plane electron effective mass $m^*$ = 0.14 ± 0.02$m_0$ was obtained ($m_0$ is free electron mass), which is conducive to achieving ultrahigh electron mobility[11]. Since the CBM and VBM of Bi and Se elements are mainly composed of p-orbitals, layered $Bi_2O_2Se$ crystals are considered to have strong spin-orbit interaction[46].

$Bi_2O_2Se$ is a semiconductor with a narrow bandgap (0.8 eV), which is particularly valuable for infrared optoelectronic devices. Chen *et al.* also conducted systematic theoretical and experimental studies on the electronic structures of $Bi_2O_2Se$ and plotted the integral band structure of $Bi_2O_2Se$ by combining scanning tunneling microscope (STM) and angle-resolved photoelectron spectroscopy (ARPES), the bandgap from both STM and ARPES exhibited excellent spatial uniformity and robustness[37]. However, although the crystal structure of $Bi_2O_2Se$ did not change under the influence of high pressure 4 GPa, the electronic change occurred including the crossing and anti-crossing behaviors of the top and the second top valence bands at different locations of the Bril-

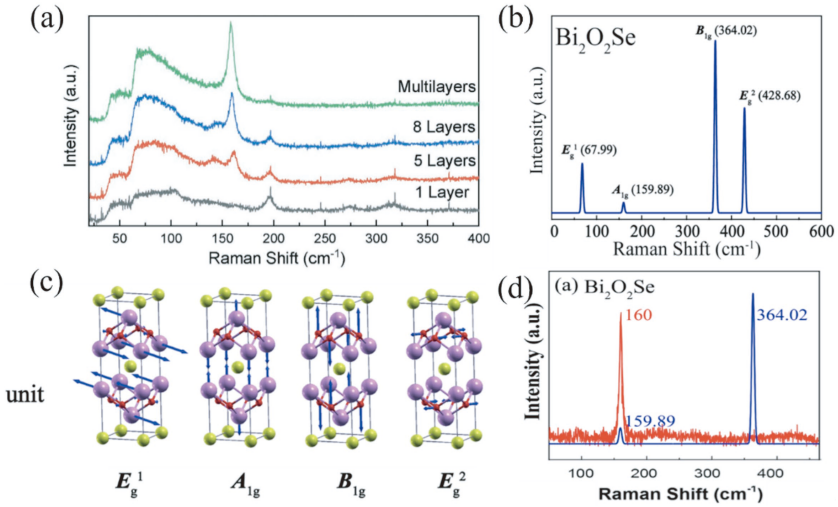


Fig. 5. (Color online) (a) Raman spectra of $Bi_2O_2Se$ films with different layers. Reproduced with permission[20]. Copyright 2019, Wiley-VCH. (b–d) Four Raman vibration modes of $Bi_2O_2Se$. Reproduced with permission[55]. Copyright 2018, American Chemical Society.

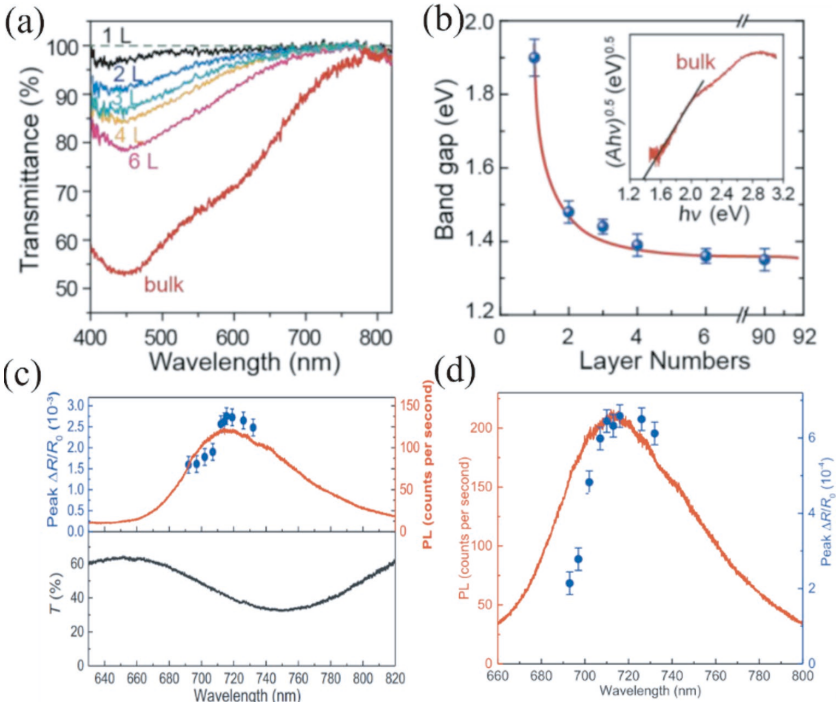


Fig. 6. (Color online) (a, b) Transmittance and band gap of 2D $Bi_2O_2Se$ films and bulk. Reproduced with permission[31]. Copyright 2017, American Chemical Society. (c) Peak differential reflection (blue symbols) and PL (red curve) of the 13 nm nanoplate as a function of the probe wavelength (upper panel) and its transmittance spectrum (lower panel). Reproduced with permission[56]. Copyright 2020, Wiley-VCH. (d) Peak differential reflection (blue symbols) and PL (red curve) of the monolayer as a function of the probe wavelength. Reproduced with permission[56]. Copyright 2020, Wiley-VCH.

louin zone due to the gradual shortening and hardening of the long and weak Bi-Se bonds between layers[53].

Raman spectroscopy is a non-destructive characterization tool, which can provide important information about structure, crystallinity, strain and defects by probing specific molecular vibration modes. According to group theory, there are 10 vibration modes based on the I4/mmm space group of $Bi_2O_2Se$, among which $A_{1g}$, $B_{1g}$, and $E_g$ modes are Raman active. Khan *et al.* conducted Raman characterization for $Bi_2O_2Se$ films with different thicknesses (Fig. 5(a)), showing that $A_{1g}$ characteristic peak was located at ~159 $cm^{-1}$, and its strength decreased with the decrease of the thickness of $Bi_2O_2Se$ films[20]. No obvious Raman characteristic peaks were observed for the monolayer $Bi_2O_2Se$ films. Cheng *et al.* combined the theory and experiment to study the Raman spectrum of $Bi_2O_2Se$. Fig. 5(b) demonstrates the four Raman vibration modes of $Bi_2O_2Se$ at the Γ-point are 159.89 ($A_{1g}$), 364.02 ($B_{1g}$), 67.99 ($E_g^1$), and 428.68 $cm^{-1}$ ($E_g^2$). It can be seen in Fig. 5(c) that the $A_{1g}$ and $B_{1g}$ modes correspond to the movement of Bi and O atoms along the *Z* axis of crystallography. The vibration of Bi and O atoms in the *XY*-plane can cause two sets of degenerate $E_g$ modes[55]. Whether or not the Raman vibration modes in crystals can be observed in the experiment depends on their experimental structures and Raman tensors. For $Bi_2O_2Se$, it is difficult to measure 2D thin film on *XZ* or *YZ* plane, so only two intrinsic Raman peaks ($A_{1g}$ and

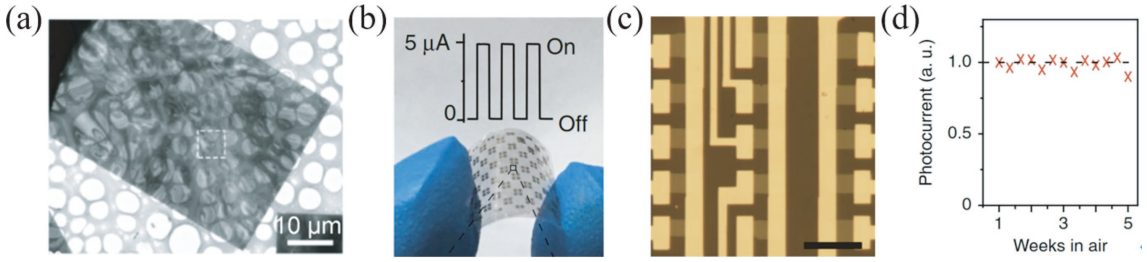


Fig. 7. (Color online) (a) TEM image of $Bi_2O_2Se$ on a copper grid. Reproduced with permission[20]. Copyright 2019, Wiley-VCH. (b) Photograph of 2D $Bi_2O_2Se$ photodetectors and arrays on mica. (c) Optical image of 3 × 5 multi-pixel array of 2D $Bi_2O_2Se$ photodetectors. (d) Photocurrent of a 2D $Bi_2O_2Se$ photodetector in air. Reproduced with permission [40]. Copyright 2018, Nature Publishing Group.

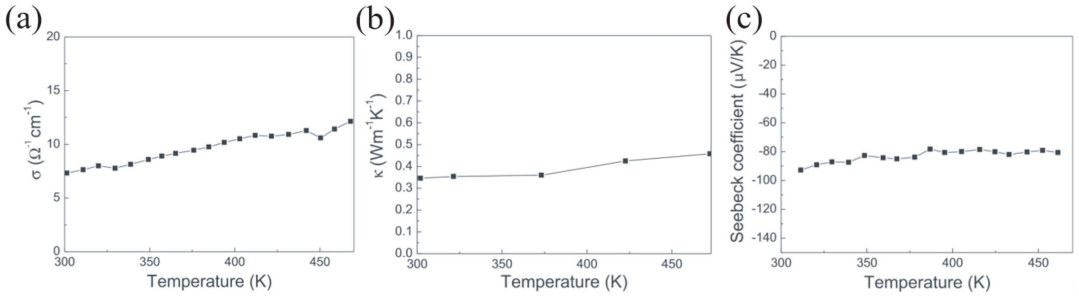


Fig. 8. (a) Electrical conductivity $\sigma$ of the $Bi_2O_2Se$ film as a function of temperature. (b) Thermal conductivity $\kappa$ of the $Bi_2O_2Se$ rectangular block as a function of temperature. (c) Seebeck coefficient $S$ of the $Bi_2O_2Se$ film as a function of temperature. Reproduced with permission[59]. Copyright 2013, Elsevier.

$B_{1g}$) can be observed. However, in the experiment, Cheng *et al.* and Pereira *et al.* did not observe the characteristic peak of $Bi_2O_2Se$ near 364 $cm^{-1}$ ($B_{1g}$) predicted by group theory and only observed the $A_{1g}$ model (about 159.2 $cm^{-1}$). As shown in Fig. 5(d), Pereira *et al.* explained the missing vibration mode of $B_{1g}$ based on the plasmon-phonon coupling $L^-$ or $L^+$ bands of $B_{1g}$ modes due to the high carrier concentration of n-type semiconductor[53, 55], just like many other highly doped semiconductors. Cheng *et al.* found that all Raman modes show redshifts under tensile strains and blueshifts under compressive strains. The $E_g$ mode exhibits to be the most sensitive mode affected by the uniaxial strain[53]. Pereira *et al.* observed the pressure evolution of the experimental low-frequency Raman-active $A_{1g}$ and $E_g$ modes. They ascribed the occurrence of several vibrational modes especially above 11.3 GPa could be related to the creation of defects in the sample[55]. Therefore, Raman spectroscopy affords a convenient and rapid means to identify the stain or defects in atomically thin film.

Light absorption is related to the band structure of semiconductors. It is helpful to study the evolution of the band structure and to extract the optical bandgap. Wu *et al.* made optical measurements on 2D $Bi_2O_2Se$ crystals with different thicknesses grown by CVD. The blue shift of the optical absorption edges occurred as the thickness decreased (Fig. 6(a)), which indicates that the bandgap increased due to the quantum size effect. By fitting the bandgap, it was found that the optical band gap can be adjusted from 1.37 to 1.90 eV as the thickness of 2D $Bi_2O_2Se$ crystals gradually changed to monolayer, as shown in Fig. 6(b)[31]. Liu *et al.* compared the results of photoluminescence, light transmission, and transient absorption spectroscopy with the electronic structure calculated by first-principles calculations. Due to the transition between the conduction band and the valence band state in the Γ valley, the multilayer $Bi_2O_2Se$ (13 nm) has a direct optical transition near 720 nm (1.7 eV), which is almost the same as the result of monolayer $Bi_2O_2Se$. Figs. 6(c) and 6(d) indicate that the electronic structure of the Γ valley does not change significantly with the change in thickness[56].

### 3.3. Mechanical property

Graphene has been proven to be one of the strongest materials ever made. The mechanical strength (stiffness) of $Bi_2O_2Se$ is also especially important for its application in various flexible functional devices. Zhang *et al.* calculated the mechanical flexibility of monolayer $Bi_2O_2Se$ with the first-principles method, the monolayer $Bi_2O_2Se$ has a greater Poisson's ratio and lower in-plane stiffness than other 2D materials (such as $MoS_2$ and graphene)[57]. In the process of characterizing the crystal structure and chemical composition for the synthesized $Bi_2O_2Se$ crystal, the $Bi_2O_2Se$ can be transferred by a polydimethylsiloxane (PDMS) and poly(methyl methacrylate) (PMMA)-assisted method onto a Cu grid for transmission electron microscope (TEM) examination, as shown in Fig. 7(a)[20]. Li *et al.* and Zhang *et al.* repeatedly measured the photoelectric properties of the $Bi_2O_2Se$ devices on a flexible substrate, and the photoelectric properties showed excellent stability[18, 41]. In addition, Yin *et al.* prepared 2D flexible $Bi_2O_2Se$ photodetectors and photodetector arrays on mica, $Bi_2O_2Se$ photodetector arrays exhibited excellent photoelectric performance and stability on a substrate with strain bending up to 1% (Figs. 7(b) and 7(d)). They showed a very stable light response within 5 weeks in the environment, proving that the 2D $Bi_2O_2Se$ photodetectors can work on a flexible substrate[40]. Chen *et al.* experimentally obtained the mechanical properties of 2D $Bi_2O_2Se$ using the nanoindentation method. Few-layer $Bi_2O_2Se$ exhibits a large intrinsic stiffness of 18–23 GPa, Young's modulus of 88.7 ± 14.4 GPa, and can withstand a high radial strain of more than 3%, demonstrating ex-

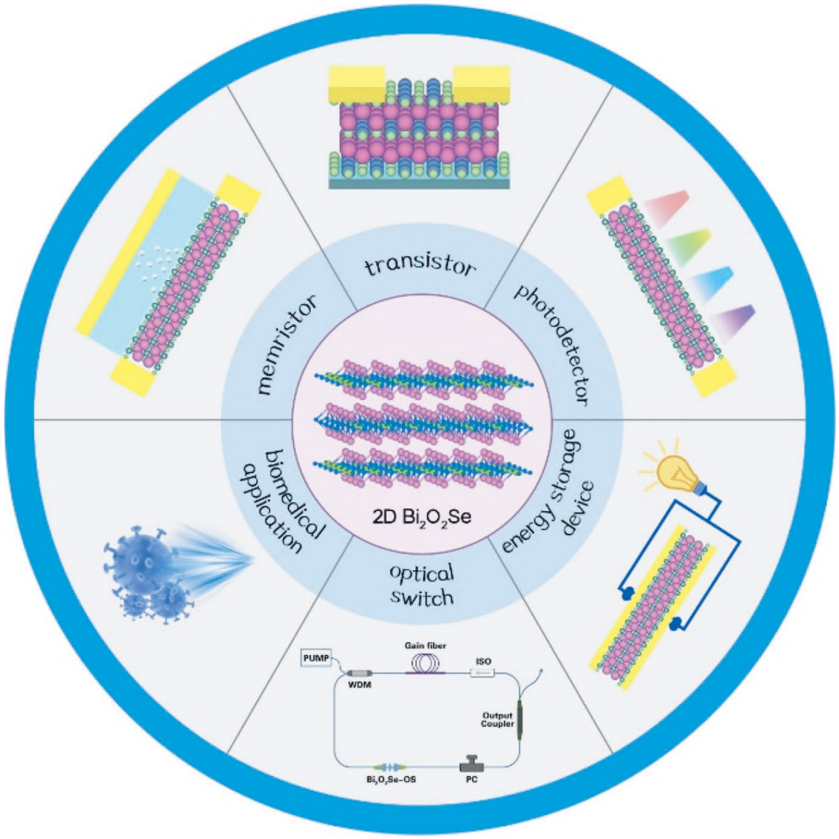


Fig. 9. (Color online) Schematic representation of device applications of $Bi_2O_2Se$.

cellent flexibility[44]. The presence of strain in 2D materials can change the band structure, carrier mobility, and so on. The strain effect is very important to understand the performance of flexible electronics. In the Raman spectrum, the stretching strain causes the Raman mode softening and red shift, while the compression strain causes the mode hardening and blue shift. The degeneracy $E_g$ modes of $Bi_2O_2Se$ split under uniaxial strain and shear strain, and the frequency variation of the degeneracy modes are anisotropic under rotating uniaxial strain[55]. In short, the excellent flexibility and stability of $Bi_2O_2Se$ thin films make it an ideal semiconductor material for flexible and wearable or printable electronic devices.

### 3.4. Thermoelectric property

$Bi_2O_2Se$ was initially investigated as a potential n-type thermoelectric material in its bulk (ceramic) form[58]. Zhang *et al.* measured the electrical conductivity, thermal conductivity, and Seebeck coefficient of $Bi_2O_2Se$ (65 $\mu$m) in the temperature range of 300–470 K as shown in Fig. 8. The thermal conductivity is only 0.346 W/(m·K) at 300 K[59]. The thermoelectric properties of materials are determined by their dimensionless thermoelectric ZT ($ZT = S^2\sigma T/\kappa$, $S$ is Seebeck coefficient, $\sigma$ is electrical conductivity, $T$ is temperature, and $\kappa$ is thermal conductivity). Generally, a material with $ZT > 1$ is considered to be excellent thermoelectric material. According to the investigation, the ZT value of $Bi_2O_2Se$ can reach 0.2 at 800 K[58]. However, theoretical studies have shown that the dimensionless thermoelectric ZT of p-doped $Bi_2O_2Se$ can reach 1.42 (800 K) with the in-plane strain. This can be compared with $Bi_2Te_3$, which is one of the most widely used and best thermoelectric materials. Recently, Yu *et al.* reported that the ZT value of n-doped $Bi_2O_2Se$ is as high as 3.35 at 800 K[60]. This is much higher than the ZT value (2.6) of SnSe at 923 K, which is known to be the most effective thermoelectric material[61].

The thermal transport of 2D materials is a key factor in thermal management, nanometer electronic devices, and thermoelectric devices. Yang *et al.* studied the in-plane and interfacial heat transfer and energy dissipation of 2D $Bi_2O_2Se$ by Raman spectroscopy. Due to the low phonon group velocity, large surface scattering, and strong anharmonicity of $Bi_2O_2Se$ phonons, the in-plane thermal conductivity of $Bi_2O_2Se$ thin films decreases with the decrease in thickness. When the thickness of $Bi_2O_2Se$ thin film is 8 nm, the in-plane thermal conductivity of $Bi_2O_2Se$ is as low as 0.926–0.18 W/(m·K), which is far lower than that of other 2D materials such as black phosphorus and $MoS_2$. However, contrary to the in-plane thermal conductivity coefficient, $Bi_2O_2Se$ thin films have larger interface binding energy, the thinner $Bi_2O_2Se$ has a stronger heat dissipation ability to the substrate, so its interface thermal conductivity increases as the thin films thickness decrease, reaching 21 MW/(m·K) when the thickness of $Bi_2O_2Se$ thin film is 8 nm[62]. Yang *et al.* exhibited the photo-bolometric effect in $Bi_2O_2Se$ photodetectors, which is based on temperature-induced hot carrier generation by light heating[63].

## 4. Applications

As a new 2D layered material, $Bi_2O_2Se$ has a unique crystal structure and novel electron transport properties. Studies have shown that $Bi_2O_2Se$ has ultrahigh carrier mobility, tunable bandgap, excellent thermoelectric property, perfect chemical and thermal stability, and controllable doping concentration, which are very attractive characteristics for electronic and optical applications. In the following, we present a brief review on the recent progress of $Bi_2O_2Se$ in photodetect-

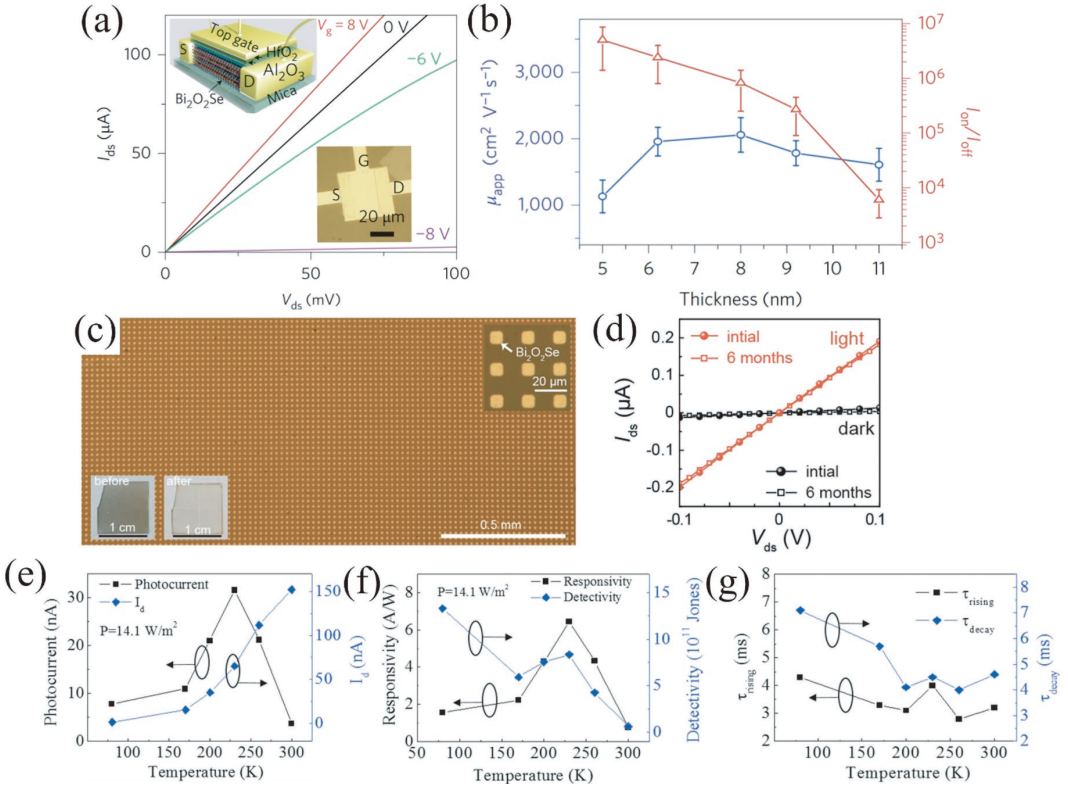


Fig. 10. (Color online) (a) Output curves of a 6.2 nm-thick $Bi_2O_2Se$ device at room temperature. (b) $\mu_{app}$ and $I_{on}/I_{off}$ of $Bi_2O_2Se$ FETs as a function of channel thickness. Reproduced with permission[11]. Copyright 2017, Nature Publishing Group. (c) OM image of centimeter-scale 2D $Bi_2O_2Se$ arrays. (d) Linear $I_{ds}$–$V_{ds}$ curves of $Bi_2O_2Se$ device with/without the illumination of 532 nm incident laser. Reproduced with permission[67]. Copyright 2017, Wiley-VCH. (e–g) Photocurrent, dark current, responsivity, detectivity, and response time as a function of temperature. Reproduced with permission[41]. Copyright 2018, Wiley-VCH.

ors, energy storage, memristors, optical switches, and biomedicine (Fig. 9).

### 4.1. Photodetectors (transistors)

The mobility of semiconductors is one of the most important parameters, which determines some key performance of electronic devices. Wu *et al.* measured the Hall mobility of $Bi_2O_2Se$ thin films at a low temperature (1.9 K) as high as 29 000 $cm^2/(V{\cdot}s)$, which is comparable to graphene[11]. The top-gated $Bi_2O_2Se$ (6.2 nm) field effect transistor (Fig. 10(a)) exhibited excellent performance at room temperature, including ultrahigh Hall mobility (up to 450 $cm^2/(V{\cdot}s)$), a high current on/off ratio (>$10^6$), and near-ideal subthreshold swing value (~65 mV/dec)[11]. In addition, the current on/off ratio and the Hall mobility of $Bi_2O_2Se$ both changed with the thickness of thin films. As the channel thickness decreased, the value of the on/off ratio increased from ~$10^3$ to ~$10^6$. For thicker $Bi_2O_2Se$, the Hall mobility at room temperature remains almost constant. However, thanks to the $Bi_2O_2Se$ thin films with a thickness of less than 6 nm, their Hall mobility would suddenly drop due to severe surface/interface scattering, as shown in Fig. 10(b)[11]. Later, Tong *et al.* reported the hall mobility of $Bi_2O_2Se$ thin film as 40 000 $cm^2/(V{\cdot}s)$ at 2 K and attributed its ultrahigh mobility to the suppressed backscattering of electrons[33]. Since the mobility is closely related to the device performance such as photoconductive gain, response speed, and so on[64, 65], it is significant to improve the mobility further by growth control, gate tuning, avoiding various scattering from the surface/interface, and surface encapsulation with a dielectric layer[66].

The preparation of $Bi_2O_2Se$ array is a prerequisite for fully exerting its potential in integrated optoelectronics and multi-pixel readout digital circuits. To this end, Wu *et al.* used diluted $H_2O_2$ and protonic mixed acid as an effective etching agent to accurately pattern the 2D semiconductor $Bi_2O_2Se$ crystal with high mobility on mica and obtained a centimeter order 2D $Bi_2O_2Se$ array. The etched 2D $Bi_2O_2Se$ crystals still retain high carrier mobility of 209 $cm^2/(V{\cdot}s)$ (room temperature), and the integrated photodetector of the prepared 2D $Bi_2O_2Se$ arrays exhibited good air stability (After being exposed to the air for about 6 months, the performance of the device hardly changed, as shown in Fig. 10(d)) and had a photoresponsivity up to 2000 A/W at 532 nm[67].

In recent decades, the near/medium infrared (IR) photodetectors have been widely used in military, academic, and commercial fields, and the semiconductor $Bi_2O_2Se$ with a narrow bandgap of about 0.8 eV is particularly valuable for IR optoelectronic detection. Up to now, many people have reported on near/medium IR optoelectronic devices. First, Li *et al.* systematically studied the near-infrared photoelectric detection performance of $Bi_2O_2Se$ thin films on mica substrate through variable temperature measurement. At 808 nm, the responsivity, detectivity, and response time reached 6.5 A/W, $8.3 \times 10^{11}$ Jones and 2.8 ms, respectively[41]. When the temperature changed from 300 to 80 K, due to the thermal radiation of carriers at low temperatures being suppressed, the carrier density was reduced, resulting in a decrease of dark current from 152 to 1.5 nA. However, the photocurrent only changed slightly, and the photoelectric performance remained basically unchanged, as shown in Figs. 10(e)–10(g), indicating that

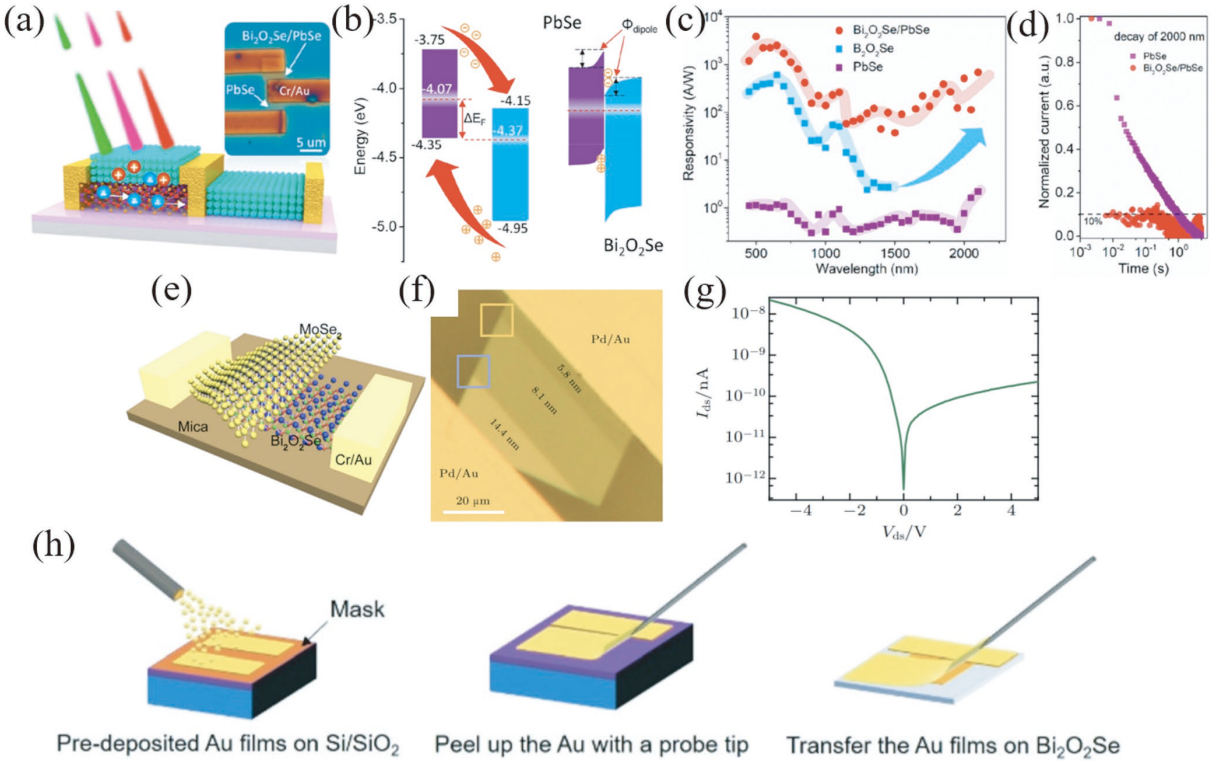


Fig. 11. (Color online) (a) Schematic illustration of the PbSe/$Bi_2O_2Se$ photodetector. (b) The estimated Type II energy band alignment between PbSe and $Bi_2O_2Se$ before and after contact based on the estimated valence band offset and work function difference in UPS. (c) Photoresponse spectra. (d) Response decay dynamics of the hybrid photodetector. Reproduced with permission[68]. Copyright 2019, American Chemical Society. (e) Schematic illustration of the $Bi_2O_2Se/MoSe_2$ heterojunction photodetector. Reproduced with permission[70]. Copyright 2019, Springer Science Business Media, LLC, part of Springer Nature. (f) OM image of as-fabricated device with 3-layered $Bi_2O_2Se$ IPJ. (g) Output characteristic curve of the device in panel (m). Reproduced with permission[71]. Copyright 2019, Chinese Physical Society. (h) Preparation of Au/$Bi_2O_2Se$/Au MSM structures on mica substrates with a probe tip. Reproduced with permission[72]. Copyright 2019, Royal Society of Chemistry.

the grown $Bi_2O_2Se$ thin films had no surface trap states and shallow defect levels. In addition, there was no significant change in device performance when exposed to air for more than three months, demonstrating good air stability of the $Bi_2O_2Se$.

Most 2D layered materials, such as graphene, TMDCs, and so on, have not yet demonstrated both high sensitivity and rapid photoelectric response in infrared detection. However, the $Bi_2O_2Se$ infrared photodetector on mica substrate reported by Yin *et al.* showed a high responsivity of 65 A/W at 1200 nm and an ultrafast response time of about 1 ps at room temperature[40]. At the same time, it exhibited a broadband optical response from visible light to 1700 nm. The photoelectric response reached 5800 A/W at 532 nm and 0.1 A/W at 1550 nm, which is comparable to other 2D materials such as graphene and TMDCs. In addition, 2D $Bi_2O_2Se$ photodetectors can be integrated on flexible substrates and have a good imaging capability[40]. Due to the inherent indirect optical bandgap of $Bi_2O_2Se$, the photoresponse performance drops sharply at $\lambda$ = 1550 nm (<0.1 A/W)[40]. To expand the $Bi_2O_2Se$ response spectrum to the wider infrared, Luo *et al.*[68] used PbSe colloidal quantum dots (CQDs) to decorate $Bi_2O_2Se$ to form a type II band structure, which facilitated the separation of photocarriers and improved the performance of $Bi_2O_2Se$ photodetectors. Schematic diagrams of the hybrid photodetector under light excitation and band structure are shown in Figs. 11(a) and 11(b), resulting in an optical response time of less than 4 ms and an infrared response greater than $10^3$ A/W at 2 $\mu$m, as shown in Figs. 11(c) and 11(d).

Compared with the monolayer or few-layer film, the multilayer film has higher state density and higher absolute light absorption, which can generate higher density photocurrent. Moreover, multilayer $Bi_2O_2Se$ has a wider spectral response than few-layer $Bi_2O_2Se$ due to the narrower bandgap. Yang *et al.* systematically studied the near-infrared photoelectric properties of multilayer $Bi_2O_2Se$ thin films with a thickness of 30 nm, which had an ultra-sensitive optical response in the range of 850–1550 nm. The responsivity, detectivity, and external quantum efficiency reach 101 A/W, $1.9 \times 10^{10}$ Jones, and 20 300% respectively at 1000 nm, and the response time is 30 ms (1500 nm)[69]. The results show that the multilayer $Bi_2O_2Se$ has higher responsivity and external quantum efficiency than the few-layer $Bi_2O_2Se$ reported in the literature[40], while maintaining a higher detectivity and a faster response time. Fu[34], Khan[20], and Tong *et al.*[33] investigated the performance of $Bi_2O_2Se$ phototransistors in the UV–Visible–NIR spectrum, the maximum value of responsivity and detectivity reached $10^5$ A/W and $10^{15}$ Jones, respectively. Yang *et al.*[70] fabricated $Bi_2O_2Se$-$MoSe_2$ photodetector as shown in Fig. 11(e). The heterostructure showed a detection range from visible light to near-infrared (405–808 nm) with response and detection efficiency of 413.1 mA/W and $3.79 \times 10^{11}$ Jones at 780 nm, respectively.

To avoid defects or contaminants generated during traditional electrode deposition or sample transfer on devices, Hong *et al.*[71] and Liu *et al.*[72] adopted different methods to

Table 2. Comparisons of device performance of $Bi_2O_2Se$ and other 2D materials.

| Material | Laser wavelength (nm) | Responsivity (A/W) | Detectivity (Jones) | Rise/decaytime (ms) | Ref. |
|---|---|---|---|---|---|
| $Bi_2O_2Se$ | 360 | 75.14 | $3.32\times10^{12}$ | 78.85 | [48] |
| $Bi_2O_2Se$ | 405 | 50055 | $8.2\times10^{12}$ | 0.032/0.098 | [33] |
| $Bi_2O_2Se$ | 450 | 60 | $2.4\times10^{10}$ | 5/7 (532 nm) | [47] |
| $Bi_2O_2Se$ | 473 | 722.2 | $5.64\times10^{11}$ | 0.267/1.1 | [73] |
| $Bi_2O_2Se$ | 532 | 842.91 | $8.18\times10^{12}$ | – | [49] |
| $Bi_2O_2Se$ | 532 | 35000 | $9\times10^{13}$ | 0.308/0.448 | [34] |
| $Bi_2O_2Se$ | 532 | 45800 | $2.65\times10^{12}$ | 200 | [74] |
| $Bi_2O_2Se$ | 590 | $9.19\times10^{6}$ | $2.08\times10^{12}$ | 39/63 | [35] |
| $Bi_2O_2Se$ | 640 | 9.1 | $1.3\times10^{8}$ | 0.036/0.016 | [72] |
| $Bi_2O_2Se$ | 640 | 2.5 | $3.2\times10^{8}$ | 0.0025/0.0048 | [71] |
| $Bi_2O_2Se$ | 660 | 22100 | $3.4\times10^{15}$ | 6/20 | [20] |
| $Bi_2O_2Se$ | 808 | 6.5 | $8.3\times10^{11}$ | 3.2/4.6 | [41] |
| $Bi_2O_2Se$ | 900 | 101 | $1.9\times10^{10}$ | 30 | [69] |
| $Bi_2O_2Se$ | 1200 | 65 | $3\times10^{9}$ | $10^{-9}$ | [40] |
| $Bi_2O_2Se/MoSe_2$ | 780 | 0.413 | $3.7\times10^{11}$ | 0.79/0.49 (515 nm) | [70] |
| $Bi_2O_2Se/PbSe$ | 2000 | $3\times10^{3}$ | – | <4 | [68] |
| BiOCl | 250 | 35.7 | $2.2\times10^{10}$ | – | [75] |
| $FePSe_3/MoS_2$ | 265 | 33600 | $1.51\times10^{13}$ | 0.32/0.36 (637 nm) | [76] |
| $SnS_2$/Au | 532 | 1125.9 | $2.12\times10^{11}$ | 20/770 | [77] |
| Graphene | 890 | 0.5 | $7.4\times10^{9}$ | $<10^{-5}$ | [78] |
| Graphene/PbS | 600 | $5\times10^{7}$ | $7\times10^{13}$ | 10/100 (532 nm) | [64] |
| Graphene | 375–3750 | $6\times10^{4}$ (Vis)<br>0.3 (NIR)<br>0.1 (MIR) | – | $<10^{-3}$ | [65] |

improve the device structures. Hong *et al.* synthesized $Bi_2O_2Se$ thin films with different thicknesses on the steps of mica substrate to form in-plane homojunction. The device's optical image is shown in Fig. 11(f), and it exhibited a diode-like rectifying behavior with an on/off ratio of $10^2$ (Fig. 11(g)). Maximum optical response of 2.5 A/W and a response time of 4.8 $\mu$s are achieved. Liu *et al.* transferred the pre-deposited gold electrodes onto the $Bi_2O_2Se$ thin films with a probe and prepared Au/$Bi_2O_2Se$/Au MSM structures on mica substrates to form metal/semiconductor contacts (Fig. 11(h)). Under optimized annealing temperature, the maximum responsivity and response time of the device reached 9.1 A/W and 36 $\mu$s with a broadband spectral response ranging from UV to NIR (360–1090 nm). In the ultra-short channel, Yang *et al.* used the ab initio quantum transport simulation to predict the performance of $Bi_2O_2Se$ FETs. The optimized n-type and p-type $Bi_2O_2Se$ FET can meet or approach the high-performance requirements of the International Technology Roadmap for Semiconductors (ITRS)[17]. Table 2 shows the comparisons of device performance of $Bi_2O_2Se$ and other 2D materials.

### 4.2. Energy storage devices

Polymer solar cells (PSCs) have attracted much attention because of their outstanding advantages such as simple structure and preparation process, low cost, light weight, and their ability to be made into flexible devices. Recently, some 2D materials have been applied to PSC. Huang *et al.* applied high-mobility $Bi_2O_2Se$ thin films as active layers in PSCs to promote charge transfer[79]. The results show that the performance of the device has been significantly improved, the PCE of PBDB-T:ITIC-based device has increased from 10.09% (0% by weight) to 12.22% (2 wt%). The PCE of the PM6:Y6-based device reached 16.28% when 2 wt% $Bi_2O_2Se$ is introduced. The optimized ternary device shows good air stability, indicating that the $Bi_2O_2Se$ material has a good application prospect in photovoltaic devices (Fig. 12).

### 4.3. Memristors

With the rapid expansion of data information, modern computers based on the von Neumann architecture are facing severe challenges. Intelligent computers that can learn, memorize and process information flexibly like the human brain are the direction and goal of future computer development. Memory resistors can remember their resistance history, which can be used on many occasions, such as nonvolatile storage devices, energy-efficient computers, neuromorphic calculating, and so on. Synapse refers to the part where neurons and neurons are connected which includes three parts: presynaptic membrane, synaptic cleft, and postsynaptic membrane[25, 80–82]. The use of memristors to simulate synapses is based on the basic idea that the electrical properties can be altered under external stimuli and then memorized similar to synaptic plasticity, which makes it possible for memristors to build brain-like large-scale integrated circuits in the future.

Recently, Zhang *et al.* used the newly emerging 2D layered semiconductor material $Bi_2O_2Se$ to realize a three-terminal memristor that simulates brain functions. Schematic diagram of the cross-sectional structure and the optical image are shown in Fig. 13[25]. Zhang *et al.* demonstrated for the first time the coexistence of long-term plasticity (LTP) and short-term plasticity (STP) by decoupling the sites where the physical LTP and STP processes occurred. The concerted action of STP and LTP can make the transient synaptic efficacy from depression to facilitation be comprehensively adjusted through stimulus frequency or intensity. Through the heuristic recurrent neural circuitry model, the complex neural process of "sleep-wake cycle autoregulation" was simulated to show the complex computing power of memristors and the

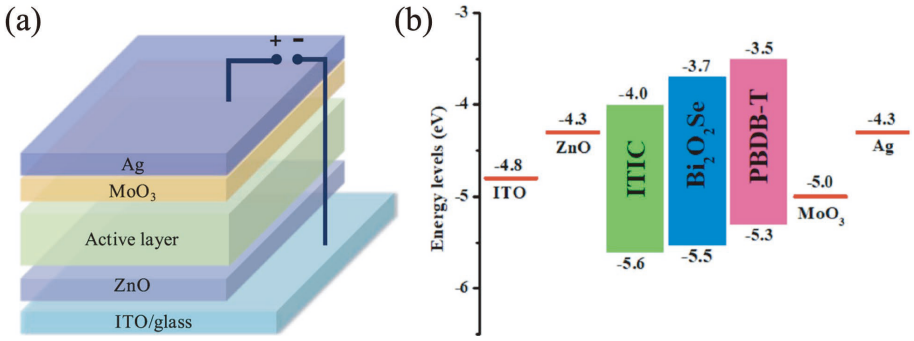


Fig. 12. (Color online) (a) Structure of polymer solar cells. (b) Energy diagram of the device. Reproduced with permission[79]. Copyright 2020, American Chemical Society.

well-designed LTP and STP[25]. This work indicates that $Bi_2O_2Se$ has great potential for complex neuromorphic functional devices for high dynamic neuromorphic computing. Furthermore, Yang *et al.*[24] developed a bidirectional all-optical synapse based on a 2D $Bi_2O_2Se$/Graphene hybrid structure. The hybrid structure presents both positive and negative photoresponsibility, which was used to realize all optically stimulated potentiation and depression. Recently, Yan *et al.* fabricate $Bi_2O_2Se$/PMN-PT 2D-FeFETs through growing high-quality $Bi_2O_2Se$ epitaxial films on ferroelectric $Pb(Mg_{1/3}Nb_{2/3})O_3$-$PbTiO_3$ (PMN-PT) single-crystal substrates. Thus, nonvolatile electric field modulation is achieved by changing the polarization direction of the ferroelectric layer, enabling the application of $Bi_2O_2Se$ in nonvolatile memory[83].

### 4.4. Optical switches

Pulsed lasers working in the mid-infrared (3–25 $\mu$m) range have broad application prospects in the fields of national defense, military, biomedical research, environmental monitoring, sensing, atmospheric communications, and imaging. So far, nonlinear optical devices with the ability to generate pulsed lasers, called passive saturable absorbers or optical switches, are one of the key factors limiting the development of mid-infrared pulsed lasers. In particular, optical switches with broadband response can produce short pulse output by rapidly switching absorption[84]. Although graphene can be used as a saturable absorber near 3 $\mu$m due to its zero bandgap, graphene has a low absorption coefficient (~2.3%) which limits its application in producing short-pulse lasers in the mid-infrared range. Therefore, finding new functional materials that can be used for mid-infrared short pulse generation is very important for the wide application of mid-infrared light sources.

Since layered $Bi_2O_2Se$ can be split along its Se plane, the surface atomic structure may be rearranged. There are nonequilibrium electrons distribution between $[Bi_2O_2]_n^{2n+}$ and $[Se]_n^{2n-}$ layer. A planar topology system can be constructed through the Majorana bound state. Nonequilibrium electrons and potential energy topological states can excite optical nonlinearities. Tian *et al.* proved that $Bi_2O_2Se$ as a saturable absorber has an ultra-wideband saturable nonlinear optical response in the wavelength range of 0.80 to 5.0 $\mu$m through Z-scan technology and pump probe technology. At 5.0 $\mu$m, the response time reaches the order of picoseconds and the response amplitude is as high as ~330.1%. An optical modulator based on 2D $Bi_2O_2Se$ semiconductor can provide a simple, low-cost, effective, and scalable nonlinear absorption material for a 3 $\mu$m Q-switched fiber laser. Fig. 14 shows a 3 $\mu$m compact fiber laser that generates laser pulses through a $Bi_2O_2Se$-based optical switch[46]. Li *et al.* have applied optical switches to the field of terahertz systems. They used a PS-assisted transfer method to transfer $Bi_2O_2Se$ to the silicon substrate to configure a $Bi_2O_2Se$/Si structured terahertz wave switch. The strong absorption of terahertz waves is caused by the accumulation of carriers at the interface. This device achieves an extinction ratio of 17.7 dB at an external laser irradiance of 1.3 W/cm$^2$ at a broadband (0.25–1.5 THz) power density and also has a switching speed of 2 MHz. This shows that $Bi_2O_2Se$ has potential for terahertz sensing, security, imaging, spectroscopy, communications, and so on[85].

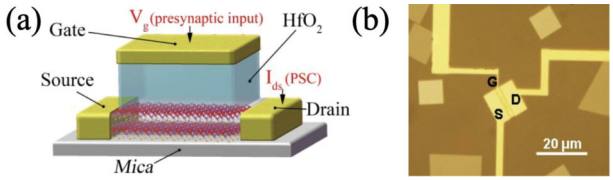


Fig. 13. (Color online) (a) Schematic diagram of the $Bi_2O_2Se$ device structure. (b) Optical image of the $Bi_2O_2Se$ memristor. Reproduced with permission[25]. Copyright 2018, Wiley-VCH.

### 4.5. Biomedical applications

Photothermal technology has always attracted much attention in the field of cancer photothermal therapy (PTT). To improve the efficiency of treatment, researchers are committed to finding suitable materials with good photothermal properties and high tissue penetration ability under near-infrared (NIR) light irradiation[86–88]. In the past decade, 2D layered materials have been developed rapidly, which promoted the development of photothermal agents such as graphene oxide (GO), $WS_2$, and $MoS_2$. It is well known that Se is a low-toxicity therapeutic agent, and Bi is beneficial to the preparation of X-ray contrast agents with good biological tolerance.

Recently, Xie *et al.*[23] synthesized $Bi_2O_2Se$ quantum dots (QDs) from bulk $Bi_2O_2Se$ crystals by a simple solution method. TEM, AFM image, and cross-sectional analysis of the synthesized $Bi_2O_2Se$ QDs are shown in Fig. 15. $Bi_2O_2Se$ QDs were used as photoacoustic (PA) imaging agents and photothermal therapy (PTT) reagents. It was confirmed that PA signal intensity increases with the increase of the concentration of QDs, and the smaller $Bi_2O_2Se$ QDs had higher photothermal conversion efficiency. The photothermal conversion coefficient of $Bi_2O_2Se$ QDs with size and thickness of 3.8 and 1.9 nm respectively is as high as 35.7%. Moreover, $Bi_2O_2Se$

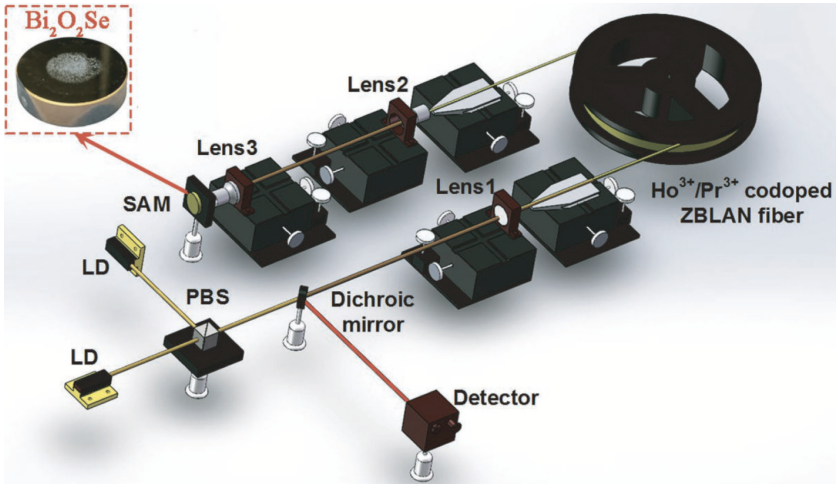


Fig. 14. (Color online) Structure diagram of a $Bi_2O_2Se$ optical switch. Reproduced with permission[46]. Copyright 2018, Wiley-VCH.

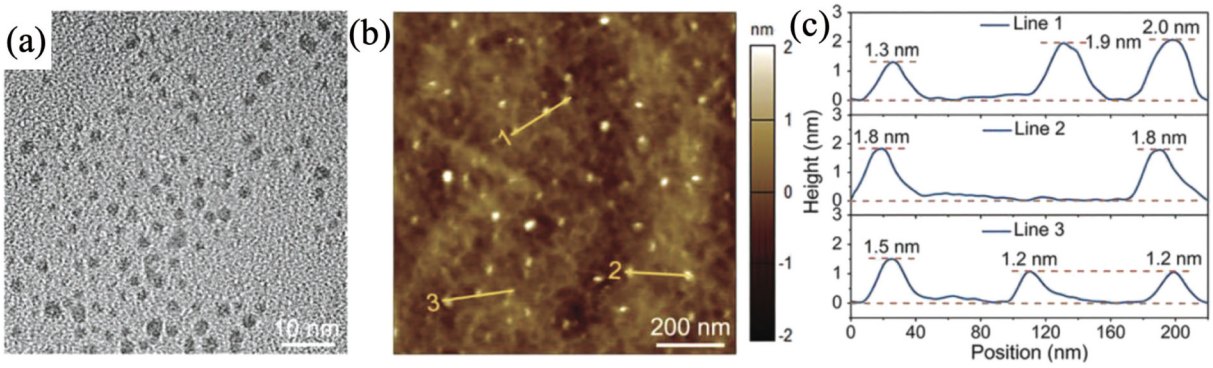


Fig. 15. (Color online) (a) TEM image, (b) AFM image, and (c) height analysis of $Bi_2O_2Se$ QDs. Reproduced with permission[23]. Copyright 2019, Wiley-VCH.

had a good photothermal stability. After four cycles of near-infrared laser irradiation, the temperature dropped only slightly (~1 °C). Experiments show that $Bi_2O_2Se$ QDs have excellent PA performance and PTT efficiency. After the injection of the drug, QDs accumulated at the tumor site, making the PA imaging of the entire tumor clearer and stronger, which is conducive to imaging-guided PTT. The drug has no obvious toxicity. More importantly, $Bi_2O_2Se$ QDs have an appropriate degradation rate in an aqueous solution, which can be almost completely degraded within 2 months. In contrast, the other two widely used inorganic PTT reagents, Au nanorods and GO nanosheets, both show high stability in aqueous solutions, indicating that they have poor degradability. Therefore, $Bi_2O_2Se$ QDs have enough stability in the body to complete the treatment and will be discharged harmlessly from the body after treatment. The results show that the biodegradable $Bi_2O_2Se$ QDs have promising application potential in imaging-guided PTT[23].

## 5. Conclusion and outlook

In summary, we reviewed the recent research progress on $Bi_2O_2Se$. The review starts from the preparation method, the preparation conditions and growth characteristics. Then, the crystal structure, electronic structure, optical properties, mechanical properties, and thermoelectric performance of $Bi_2O_2Se$ are introduced in detail. Subsequently, $Bi_2O_2Se$ applications in optoelectronics, energy storage, neuromorphic computing, nonvolatile memory, terahertz, and biomedicine were presented.

2D $Bi_2O_2Se$ has the characteristics of atomic layer thickness, ultrahigh mobility, moderate and tunable band structure, high chemical and thermal stability, and excellent mechanical flexibility. Therefore, it has quickly become a research focus since its first report by the Peng group. Its rich physical and chemical properties make $Bi_2O_2Se$ a great promising application prospect in solar cells, energy storage, environmental catalysis, sensors, memory, and so on. Although $Bi_2O_2Se$ is a new 2D material, we have seen rapid growth in research interest on it in recent years. However, there are still many challenges for its large-scale application in the future.

At present, 2D $Bi_2O_2Se$ thin films have been synthesized generally by using a bottom-up method or top-down method. Nonetheless, the controllable preparation of 2D $Bi_2O_2Se$ single crystals with large size and atomic thickness still needs further systematic study. Moreover, large-area transferring $Bi_2O_2Se$ thin films without introducing extrinsic contamination or intrinsic defects still face tough challenges[34]. In photoelectric device applications, although QDs were used to improve the photoelectric sensitivity of $Bi_2O_2Se$ photodetector, expensive production costs, complicated sensitization process, and even the heavy metal ions contained in QDs are great obstacles against putting $Bi_2O_2Se$ into practical applications. In addition, the dark current of the device after sensitization becomes substantially higher, which is unfavorable for improving the device detectivity and the signal to noise ratio[68]. In an electronic $Bi_2O_2Se$ thin film device, the heat generated

in electric measurement is not easy to be dissipated in time due to its low in-plane thermal conductivity[62]. Therefore, overheating in electrical measurement burns the device. So the fine metal-semiconductor contact and heat management need more consideration.

The photodetectors (transistors), flexible electronic devices, energy storage devices, and so on that are described in this article are only part of the $Bi_2O_2Se$ applications. The less studied and meaningful properties in 2D $Bi_2O_2Se$ such as ferroelectricity and ferroelasticity, have great promise for future research in phase change engineering, piezoelectricity, electrostriction, and so on[89, 90]. 2D $Bi_2O_2Se$ has exhibited many excellent properties and has achieved some important applications in the fields of industrial production, environment monitoring, energy harvesting and medical treatment. However, the properties and application of $Bi_2O_2Se$ still have a big room to be explored and more wonderful performance is expected in future research work.

## Acknowledgements

This work is supported by China University of Geosciences (Beijing) College Students' Innovative Entrepreneurial Training Plan Program(No. 202211415026). National Natural Science Foundation of China (No. 11974318). China University of Geosciences (Beijing) 2021 Undergraduate Education Quality Improvement Plan Construction Project (No. XNFZ202106).

## References

[1] Lopez-Sanchez O, Lembke D, Kayci M, et al. Ultrasensitive photodetectors based on monolayer $MoS_2$. Nat Nanotechnol, 2013, 8, 497
[2] Zhang W J, Huang J K, Chen C H, et al. High-gain phototransistors based on a CVD $MoS_2$ monolayer. Adv Mater, 2013, 25, 3456
[3] Chang Y H, Zhang W J, Zhu Y H, et al. Monolayer $MoSe_2$ grown by chemical vapor deposition for fast photodetection. ACS Nano, 2014, 8, 8582
[4] Anichini C, Czepa W, Pakulski D, et al. Chemical sensing with 2D materials. Chem Soc Rev, 2018, 47, 4860
[5] Xu S P, Fu H X, Tian Y, et al. Exploiting two-dimensional $Bi_2O_2Se$ for trace oxygen detection. Angew Chem Int Ed, 2020, 59, 17938
[6] Shehzad K, Shi T J, Qadir A, et al. Environmental sensing: Designing an efficient multimode environmental sensor based on graphene-silicon heterojunction. Adv Mater Technol, 2017, 2, 1600262
[7] Li J F, Liang Z Z, Wang Y F, et al. Enhanced efficiency of polymer solar cells through synergistic optimization of mobility and tuning donor alloys by adding high-mobility conjugated polymers. J Mater Chem C, 2018, 6, 11015
[8] Vu Q A, Kim H, Nguyen V L, et al. Memristors: A high-on/off-ratio floating-gate memristor array on a flexible substrate via CVD-grown large-area 2D layer stacking. Adv Mater, 2017, 29, 1703363
[9] Novoselov K S, Geim A K, Morozov S V, et al. Electric field effect in atomically thin carbon films. Science, 2004, 306, 666
[10] Brown A, Rundqvist S. Refinement of the crystal structure of black phosphorus. Acta Cryst, 1965, 19, 684
[11] Wu J X, Yuan H T, Meng M M, et al. High electron mobility and quantum oscillations in non-encapsulated ultrathin semiconducting $Bi_2O_2Se$. Nat Nanotechnol, 2017, 12, 530
[12] Zhao Y T, Wang H Y, Huang H, et al. Back cover: Surface coordination of black phosphorus for robust air and water stability (Angew. Chem. Int. Ed. 16/2016). Angew Chem Int Ed, 2016, 55, 5097
[13] Mak K F, Lee C, Hone J, et al. Atomically thin $MoS_2$: A new direct-gap semiconductor. Phys Rev Lett, 2010, 105, 136805
[14] Li L K, Yu Y J, Ye G J, et al. Black phosphorus field-effect transistors. Nat Nanotechnol, 2014, 9, 372
[15] Radisavljevic B, Radenovic A, Brivio J, et al. Single-layer $MoS_2$ transistors. Nat Nanotechnol, 2011, 6, 147
[16] Wei Q, Li R, Lin C, et al. Quasi-two-dimensional se-terminated bismuth oxychalcogenide ($Bi_2O_2Se$). ACS Nano, 2019, 13, 13439
[17] Yang J, Quhe R, Li Q, et al. Sub 10 nm bilayer $Bi_2O_2Se$ transistors. Adv Electron Mater, 2019, 5, 1800720
[18] Zhang C, Wu J, Sun Y, et al. High-mobility flexible oxyselenide thin-film transistors prepared by a solution-assisted method. J Am Chem Soc, 2020, 142, 2726
[19] Tan C, Tang M, Wu J, et al. Wafer-Scale growth of single-crystal 2D semiconductor on perovskite oxides for high-performance transistors. Nano Lett, 2019, 19, 2148
[20] Khan U, Luo Y, Tang L, et al. Controlled vapor–solid deposition of millimeter-size single crystal 2D $Bi_2O_2Se$ for high-performance phototransistors. Adv Funct Mater, 2019, 29, 1807979
[21] Chen G, Wu J, Wang B, et al. High-performance self-powered photodetector based on $Bi_2O_2Se$ nanosheets. Appl Phys A, 2020, 126, 579
[22] Xu R, Wang S, Li Y, et al. Layered semiconductor $Bi_2O_2Se$ for broadband pulse generation in the near-infrared. IEEE Photonics Technol Lett, 2019, 31, 1056
[23] Xie H H, Liu M Q, You B H, et al. Photothermal therapy: Biodegradable $Bi_2O_2Se$ quantum dots for photoacoustic imaging-guided cancer photothermal therapy. Small, 2020, 16, 2070013
[24] Yang C, Chen T, Verma D, et al. Bidirectional all-optical synapses based on a 2D $Bi_2O_2Se$/graphene hybrid structure for multifunctional optoelectronics. Adv Funct Mater, 2020, 30, 2001598
[25] Zhang Z Y, Li T R, Wu Y J, et al. Truly concomitant and independently expressed short-and long-term plasticity in a $Bi_2O_2Se$-based three-terminal memristor. Adv Mater, 2019, 31, 1805769
[26] Allen M J, Tung V C, Kaner R B. Honeycomb carbon: A review of graphene. Chem Rev, 2010, 110, 132
[27] Huang X, Zeng Z Y, Zhang H. Metal dichalcogenide nanosheets: Preparation, properties and applications. Chem Soc Rev, 2013, 42, 1934
[28] Nicolosi V, Chhowalla M, Kanatzidis M G, et al. Liquid exfoliation of layered materials. Science, 2013, 340, 1226419
[29] Huang Y, Pan Y H, Yang R, et al. Universal mechanical exfoliation of large-area 2D crystals. Nat Commun, 2020, 11, 2453
[30] Fu Q, Dai J Q, Huang X Y, et al. One-step exfoliation method for plasmonic activation of large-area 2D crystals. Adv Sci, 2022, 2204247
[31] Wu J X, Tan C W, Tan Z J, et al. Controlled synthesis of high-mobility atomically thin bismuth oxyselenide crystals. Nano Lett, 2017, 17, 3021
[32] Wu J X, Qiu C G, Fu H X, et al. Low residual carrier concentration and high mobility in 2D semiconducting $Bi_2O_2Se$. Nano Lett, 2019, 19, 197
[33] Tong T, Chen Y F, Qin S C, et al. Sensitive and ultrabroadband phototransistor based on two-dimensional $Bi_2O_2Se$ nanosheets. Adv Funct Mater, 2019, 29, 1905806
[34] Fu Q D, Zhu C, Zhao X X, et al. Ultrasensitive 2D $Bi_2O_2Se$ phototransistors on silicon substrates. Adv Mater, 2019, 31, 1804945
[35] Khan U, Tang L, Ding B F, et al. Nanoribbons: Catalyst-free growth of atomically thin $Bi_2O_2Se$ nanoribbons for high-performance electronics and optoelectronics. Adv Funct Mater, 2021, 31, 2170230
[36] Avishan N, Hussain N, Nosheen F. Large-scale graphene production and transfer for industrial applications. MaterInnov, 2022, 2, 15
[37] Chen C, Wang M X, Wu J X, et al. Electronic structures and unusually robust bandgap in an ultrahigh-mobility layered oxide semiconductor, $Bi_2O_2Se$. Sci Adv, 2018, 4, eaat8355
[38] Zeng T, You Y C, Wang X F, et al. Chemical vapor deposition and

device application of two-dimensional molybdenum disulfide-based atomic crystals. Prog Chem, 2016, 28, 459

[39] Yu J X, Li J, Zhang W F, et al. Synthesis of high quality two-dimensional materials *via* chemical vapor deposition. Chem Sci, 2015, 6, 6705

[40] Yin J B, Tan Z J, Hong H, et al. Ultrafast and highly sensitive infrared photodetectors based on two-dimensional oxyselenide crystals. Nat Commun, 2018, 9, 3311

[41] Li J, Wang Z X, Wen Y, et al. High-performance near-infrared photodetector based on ultrathin $Bi_2O_2Se$ nanosheets. Adv Funct Mater, 2018, 28, 1706437

[42] Fu H X, Wu J X, Peng H L, et al. Self-modulation doping effect in the high-mobility layered semiconductor $Bi_2O_2Se$. Phys Rev B, 2018, 97, 241203

[43] Wu Z, Liu G L, Wang Y X, et al. Seed-induced vertical growth of 2D $Bi_2O_2Se$ nanoplates by chemical vapor transport. Adv Funct Mater, 2019, 29, 1906639

[44] Chen W J, Khan U, Feng S M, et al. High-fidelity transfer of 2D $Bi_2O_2Se$ and its mechanical properties. Adv Funct Mater, 2020, 30, 2004960

[45] Zhang X, Liu Y F, Zhang G H, et al. Thermal decomposition of bismuth oxysulfide from photoelectric $Bi_2O_2S$ to superconducting $Bi_4O_4S_3$. ACS Appl Mater Interfaces, 2015, 7, 4442

[46] Tian X L, Luo H Y, Wei R F, et al. Pulsed lasers: An ultrabroadband mid-infrared pulsed optical switch employing solution-processed bismuth oxyselenide. Adv Mater, 2018, 30, 1870233

[47] Yang X, Zhang Q, Song Y C, et al. High mobility two-dimensional bismuth oxyselenide single crystals with large grain size grown by reverse-flow chemical vapor deposition. ACS Appl Mater Interfaces, 2021, 13, 49153

[48] Li M Q, Dang l L Y, Wang G G, et al. Bismuth oxychalcogenide nanosheet: Facile synthesis, characterization, and photodetector application. Adv Mater Technol, 2020, 5, 2000180

[49] Dang L Y, Liu M Q, Wang G G, et al. Organic ion template-guided solution growth of ultrathin bismuth oxyselenide with tunable electronic properties for optoelectronic applications. Adv Funct Mater, 2022, 32, 2201020

[50] Tong T, Zhang M H, Chen Y Q, et al. Ultrahigh Hall mobility and suppressed backward scattering in layered semiconductor $Bi_2O_2Se$. Appl Phys Lett, 2018, 113, 072106

[51] Williams M L. CRC handbook of chemistry and physics. 76th ed. Occup Environ Med, 1996, 53, 504

[52] Horák J, Stary Z, Lošťák P, et al. Anti-site defects in n-$Bi_2Se_3$ crystals. J Phys Chem Solids, 1990, 51, 1353

[53] Pereira A L J, Santamaría-Pérez D, Vilaplana R, et al. Experimental and theoretical study of $SbPO_4$ under compression. Inorg Chem, 2020, 59, 287

[54] Pan X, Chen H X, Lu L, et al. Incorporating guanidinium as perovskitizer-cation of two-dimensional metal halide for crystal-array photodetectors. Chem Asian J, 2021, 16, 1925

[55] Cheng T, Tan C W, Zhang S Q, et al. Raman spectra and strain effects in bismuth oxychalcogenides. J Phys Chem C, 2018, 122, 19970

[56] Liu S Y, Tan C W, He D W, et al. Optical properties and photocarrier dynamics of $Bi_2O_2Se$ monolayer and nanoplates. Adv Optical Mater, 2020, 8, 1901567

[57] Zhang Y, Gao Q, Han X Y, et al. Mechanical flexibility and strain engineered-band structures of monolayer $Bi_2O_2Se$. Phys E, 2020, 116, 113728

[58] Guo D L, Hu C G, Xi Y, et al. Strain effects to optimize thermoelectric properties of doped $Bi_2O_2Se$ via tran-blaha modified becke-Johnson density functional theory. J Phys Chem C, 2013, 117, 21597

[59] Zhang K Y, Hu C G, Kang X L, et al. Synthesis and thermoelectric properties of $Bi_2O_2Se$ nanosheets. Mater Res Bull, 2013, 48, 3968

[60] Yu J B, Sun Q. $Bi_2O_2Se$ nanosheet: An excellent high-temperature n-type thermoelectric material. Appl Phys Lett, 2018, 112, 053901

[61] Zhao L D, Lo S H, Zhang Y S, et al. Ultralow thermal conductivity and high thermoelectric figure of merit in SnSe crystals. Nature, 2014, 508, 373

[62] Yang F, Wang R D, Zhao W W, et al. Thermal transport and energy dissipation in two-dimensional $Bi_2O_2Se$. Appl Phys Lett, 2019, 115, 193103

[63] Yang H, Tan C W, Deng C Y, et al. Bolometric effect in $Bi_2O_2Se$ photodetectors. Small, 2019, 15, e1904482

[64] Konstantatos G, Badioli M, Gaudreau L, et al. Hybrid graphene–quantum dot phototransistors with ultrahigh gain. Nat Nanotechnol, 2012, 7, 363

[65] Liu W, Lv J H, Peng L, et al. Graphene charge-injection photodetectors. Nat Electron, 2022, 5, 281

[66] Wang L, Meric I, Huang P Y, et al. One-dimensional electrical contact to a two-dimensional material. Science, 2013, 342, 614

[67] Wu J, Liu Y, Tan Z, et al. Chemical patterning of high-mobility semiconducting 2D $Bi_2O_2Se$ crystals for integrated optoelectronic devices. Adv Mater, 2017, 29, 1704060

[68] Luo P, Zhuge F W, Wang F K, et al. PbSe quantum dots sensitized high-mobility $Bi_2O_2Se$ nanosheets for high-performance and broadband photodetection beyond 2 μm. ACS Nano, 2019, 13, 9028

[69] Yang H, Chen W, Zheng X M, et al. Near-infrared photoelectric properties of multilayer $Bi_2O_2Se$ nanofilms. Nanoscale Res Lett, 2019, 14, 371

[70] Yang T, Li X, Wang L M, et al. Broadband photodetection of 2D $Bi_2O_2Se$-$MoSe_2$ heterostructure. J Mater Sci, 2019, 54, 14742

[71] Hong C Y, Huang G F, Yao W W, et al. Thickness-modulated in-plane $Bi_2O_2Se$ homojunctions for ultrafast high-performance photodetectors. Chin Phys B, 2019, 28, 367

[72] Liu X L, Li R P, Hong C Y, et al. Highly efficient broadband photodetectors based on lithography-free Au/$Bi_2O_2Se$/Au heterostructures. Nanoscale, 2019, 11, 20707

[73] Li J, Wang Z X, Chu J W, et al. Oriented layered $Bi_2O_2Se$ nanowire arrays for ultrasensitive photodetectors. Appl Phys Lett, 2019, 114, 151104

[74] Li D Y, Han X, Xu G Y, et al. $Bi_2O_2Se$ photoconductive detector with low power consumption and high sensitivity. Acta Phys Sin Chin Ed, 2020, 69, 248502

[75] Han W, Li C, Yang S J, et al. Atomically thin oxyhalide solar-blind photodetectors. Small, 2020, 16, e2000228

[76] Long M S, Shen Z, Wang R J, et al. Ultrasensitive solar-blind ultraviolet photodetector based on $FePSe_3$/$MoS_2$ heterostructure response to 10.6 μm. Adv Funct Mater, 2022, 32, 2204230

[77] Han X, Xing J, Xu H, et al. Remarkable improved photoelectric performance of $SnS_2$ field-effect transistor with Au plasmonic nanostructures. Nanotechnology, 2020, 31, 215201

[78] Xu Y, Ali A, Shehzad K, et al. Photodetectors: Solvent-based soft-patterning of graphene lateral heterostructures for broadband high-speed metal-semiconductor-metal photodetectors. Adv Mater Technol, 2017, 2, 1600241

[79] Huang C W, Yu H. 2D $Bi_2O_2Se$ with high mobility for high performance polymer solar cells. ACS Appl Mater Interfaces, 2020, 12, 19643

[80] Ding G L, Yang B D, Chen R S, et al. Reconfigurable 2D $WSe_2$-based memtransistor for mimicking homosynaptic and heterosynaptic plasticity. Small, 2021, 17, 2170213

[81] Du J Y, Ge C, Riahi H, et al. Dual-gated $MoS_2$ transistors for synaptic and programmable logic functions. Adv Electron Mater, 2020, 6, 1901408

[82] Yang Q Y, Luo Z D, Zhang D W, et al. Controlled optoelectronic response in van der Waals heterostructures for In-sensor computing. Adv Funct Mater, 2022, 32(45), 202207290

[83] Yan J M, Ying J S, Yan M Y, et al. Optoelectronic coincidence detection with two-dimensional $Bi_2O_2Se$ ferroelectric field-effect tran-

sistors. Adv Funct Mater, 2021, 31, 2103982
[84] Wang F K, Yang S J, Wu J, et al. Emerging two-dimensional bismuth oxychalcogenides for electronics and optoelectronics. InfoMat, 2021, 3, 1251
[85] Li Z W, Li J S. $Bi_2O_2Se$ for broadband terahertz wave switching. Appl Opt, 2020, 59, 11076
[86] Meng X D, Liu Z Q, Cao Y, et al. Cancer therapy: Fabricating aptamer-conjugated PEGylated-$MoS_2$/$Cu_{1.8}S$ theranostic nanoplatform for multiplexed imaging diagnosis and chemo-photothermal therapy of cancer. Adv Funct Mater, 2017, 27, 1605592
[87] Chen Z, Zhao P F, Luo Z Y, et al. Cancer cell membrane-biomimetic nanoparticles for homologous-targeting dual-modal imaging and photothermal therapy. ACS Nano, 2016, 10, 10049
[88] Li B, Yuan F K, He G J, et al. Ultrasmall $CuCo_2S_4$ nanocrystals: All-in-one theragnosis nanoplatform with magnetic resonance/near-infrared imaging for efficiently photothermal therapy of tumors. Adv Funct Mater, 2017, 27, 1606218
[89] Wu M H, Zeng X C. Bismuth oxychalcogenides: A new class of ferroelectric/ferroelastic materials with ultra high mobility. Nano Lett, 2017, 17, 6309
[90] Zhu Z Y, Yao X P, Zhao S, et al. Giant modulation of the electron mobility in semiconductor $Bi_2O_2Se$ via incipient ferroelectric phase transition. J Am Chem Soc, 2022, 144, 4541

**Huayu Tao** is an undergraduate in the School of Materials Science and Engineering of China University of Geosciences (Beijing), mainly engaged in the research of low dimensional oxide materials. Her work has been published in Renewable & Sustainable Energy Reviews.

**Gengwei Li** has worked in China University of Geosciences (Beijing) since he graduated from Beijing Normal University with a master's degree in optics in 2001, and received a doctorate in solid geophysics from China University of Geosciences (Beijing) in 2013. Mainly engaged in the theoretical research of optics, thin film materials and electromagnetic fields. Nearly 50 papers have been published, including Materials Research Express, Acta Physica Sinica, Materials Review, OptoElectronics Letters, etc.